Proceedings of PVP2007
2007 ASME Pressure Vessels and Piping Division Conference
July 22-26, 2007, San Antonio, Texas

PVP2007-26440

RATCHETING OF STAINLESS STEEL 304 UNDER MULTIAXIAL NONPROPORTIONAL LOADING

Kwang S. Kim
Department of Mechanical Engineering, Pohang University of Science and Technology, Pohang 790-784, Korea

Rong Jiao
Department of Aerospace and Engineering Mechanics, University of Texas, Austin, Texas 78712, U.S.A.

Xu Chen
School of Chemical Engineering and Technology, Tianjin University, Tianjin 30072, China

Masao Sakane
Department of Mechanical Engineering, Ritsumeikan University, Kasatsu-shi, Shiga 525-8577, Japan

ABSTRACT

Ratcheting tests are conducted on stainless steel 304 under uniaxial, torsional, and combined axial-torsional loading. The ratcheting strain is predicted based on the constitutive theory that incorporates a modified Ohno-Wang kinematic hardening rule and Tanaka's isotropic hardening model. The results show that the main features of the stress-strain response can be simulated with the constitutive model. The experimental and predicted ratcheting strains for nonproportional paths are found in decent correlation. Ratcheting strain depends highly on the loading path and load level, and less on cyclic hardening or softening of the material. The torsional ratcheting strain under mean shear stress with (or without) fully reversed axial strain cycling is found close to the axial ratcheting strain under equivalent mean stress with (or without) torsional strain cycling.

INTRODUCTION

Ratcheting is a phenomenon in which plastic strain is accumulated under cyclic loading with mean stress. Increasing ratcheting strain will accelerate fatigue damage, eventually leading to failure of the material. For its implication on the safety of engineering components there has been an abundance of studies, both experimental and analytical, on the ratcheting behavior of engineering materials. Many analytical models have been proposed for predicting ratcheting, see [1, 2] for a review. Most of the models are based on the Armstrong-Frederick kinematic hardening rule [3] with some modification of the dynamic recovery term. The Ohno-Wang model [4] is one of these models, where the critical state and power function introduced in the dynamic recovery term enables to predict uniaxial ratcheting successfully. However, it overpredicts multiaxial ratcheting almost always. Consequently, many modified models have emerged. Chen et al. [5]'s model is one of them. In these modified models the efforts are usually placed on controlling ratcheting through a proper assessment of the nonproportional loading effect in nonlinear kinematic hardening models. These modifications usually generate better correlation as a whole, but not for all loading paths. The material is usually assumed cyclically stable. The inclusion of isotropic hardening in multiaxial ratcheting analysis is found only in a small number of studies. The ratcheting simulation is often limited to a small number of cycles where the cyclic change of the material is still in progress. Thus, it appears desirable to include isotropic hardening capability in the model for more meaningful comparison with experimental data.

The additional hardening in stainless steels under nonproportional cyclic loading has been extensively studied and a large body of literature exists. In the framework of flow theories of plasticity or viscoplasticity, additional hardening is usually described by nonproportional loading parameters together with relevant evolution equations. The constitutive models in this category include Calloch and Marquis[6], Tanaka[7], among others.

The objective of this study is to investigate the ratcheting behavior of stainless steel 304 by performing axial-torsional cyclic tests and evaluate a predictive method based on Chen et al.'s model [5] extended to include the effect of cyclic hardening/softening and additional hardening under nonproportional loading. The isotropic hardening model employed in this study is Tanaka's model [7] to be outlined later. The predicted constitutive response and ratcheting strain will be compared with experimental data for uniaxial, torsional, and a few nonproportional axial-torsional cycles.

EXPERIMENT

The test material, stainless steel 304, was acquired in the form of a round bar with a diameter of 32mm. The chemical composition of the material is (wt.%): C 0.05, Si 0.38, P 0.0274, S 0.025, Ni 9.018, Cr 18.417, Mo 0.206, Cu 0.411, V 0.05, N 0.0626. The tensile stress-strain curve is given in Fig. 1. Cylindrical specimens with outer and inner diameters of 12.5mm and 10mm, respectively, were used in the tests. Tests were conducted on an Instron tension-torsion machine using a biaxial extensometer mounted on the outside of the specimen gage section. The strain rate of strain-controlled cycling was $2\times10^{-3}/\mathrm{s}$, and the stress rate of stress-controlled cycling was $50\mathrm{MPa}/\mathrm{s}$. All tests were conducted at room temperature. Tests carried out are as follows:

(1) Uniaxial ($\Delta\varepsilon/2$ =0.4%, 1.6%, 2.0%), torsional ($\Delta\varepsilon_{eq}/2=0.8\%$), and circular path tests ($\Delta\varepsilon_{eq}/2=0.4\%$, 0.8%, 1.2%) under fully reversed strain control,

(2) Uniaxial ratcheting tests ($\Delta\sigma/2$ = 235MPa, σ_{mean} =235MPa; $\Delta\sigma/2$ = 200MPa, σ_{mean} =200MPa),

(3) Torsional ratcheting test ($\Delta\sigma_{eq}$ =235MPa, $(\sigma_{mean})_{eq}$ =235MPa),

(4) Axial-torsional ratcheting tests with loading paths as given in Fig. 2. Case 1 – Case 5 were conducted under axial stress control and torsional strain control. Case 6 was carried out under torsional stress control and axial strain control. The details of these tests are specified in Table 1. It is noted the equivalent stress and strain are, respectively, defined by $\sigma_{eq}=(\sigma^2+3\tau^2)^{1/2}$, $\varepsilon_{eq}=(\varepsilon^2+\gamma^2/3)^{1/2}$, where σ, τ, ε, γ are the usual axial and shear stresses and strains.

TABLE 1. LOADING CONDITIONS FOR MULTIAXIAL RATCHETING TESTS

Path type	Test no.	σ_{mean} (MPa)	$\Delta\sigma/2$ (MPa)	$\Delta\gamma/2$ (%)	γ_{mean} (%)
Case 1	1	100	0	0.866	0
Case 1	2	150	0	0.866	0
Case 2	1	100	100	0.866	0
Case 2	2	75	75	0.866	0
Case 3		100	100	0.866	0
Case 4		100	100	0.866	0
Case 5		100	100	0.866	0
Case 6	$\sqrt{3}\tau_{mean}=100MPa$, $\sqrt{3}\Delta\tau/2=0$, $\Delta\varepsilon/2=0.5$, $\varepsilon_{mean}=0$				

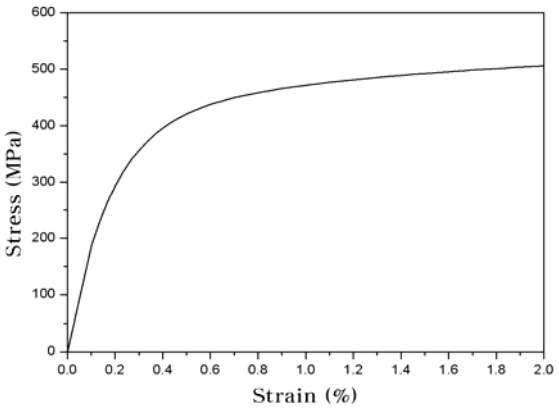

FIG. 1 TENSILE STRESS-STRESS CURVE OF STAINLESS STEEL 304

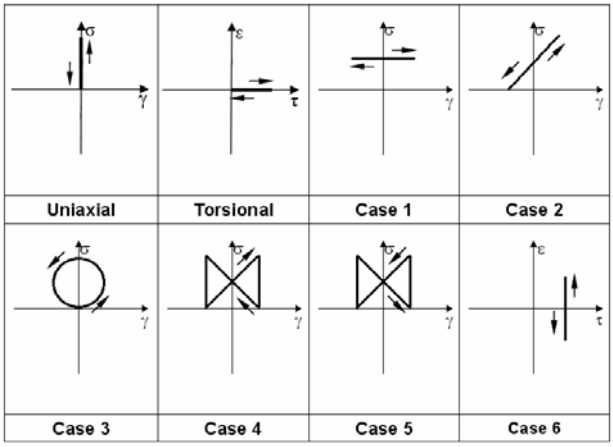

FIG. 2 LOADING PATHS FOR RATCHETING TESTS

CONSTITUTIVE MODEL

The constitutive model used in this study is outlined in the following:

Flow rule and yield surface

The total strain increment is decomposed into elastic and plastic parts:

$$d\boldsymbol{\varepsilon}=d\boldsymbol{\varepsilon}_e+d\boldsymbol{\varepsilon}_p, \tag{1}$$

where the elastic strain $\boldsymbol{\varepsilon}_e$ is related to stress $\boldsymbol{\sigma}$ by Hooke's law:

$$\boldsymbol{\varepsilon}_e=\frac{1+\nu}{E}\boldsymbol{\sigma}-\frac{\nu}{E}(tr\boldsymbol{\sigma})I, \tag{2}$$

where E and ν are Young's modulus and Poisson's ratio, respectively. The plastic strain increment $d\boldsymbol{\varepsilon}_p$ follows the flow rule given by:

$$d\boldsymbol{\varepsilon}_p = \frac{1}{H_p}\langle d\boldsymbol{s} : \boldsymbol{n}\rangle \boldsymbol{n} . \tag{3}$$

In equations (2) and (3), $\boldsymbol{s}$ is the deviatoric stress tensor, i.e. $\boldsymbol{s} = \boldsymbol{\sigma} - 1/3 tr(\boldsymbol{\sigma})\boldsymbol{I}$, $\boldsymbol{I}$ is the unit tensor and $tr(\boldsymbol{\sigma})$ is the trace of $\boldsymbol{\sigma}$, the inner product is defined by $\boldsymbol{s} : \boldsymbol{t} = s_{ij}t_{ij}$, H_p is the plastic modulus determined by the flow rule, the hardening rule and the consistence condition, $\boldsymbol{n}$ is the outward normal to the yield surface:

$$\boldsymbol{n} = \sqrt{\frac{3}{2}}\frac{\boldsymbol{s} - \boldsymbol{\alpha}}{\sigma}, \tag{4}$$

and the symbol $\langle\ \rangle$ denotes MacCauley's bracket: $\langle A\rangle = A$ if $A > 0$, $\langle A\rangle = 0$ otherwise.

The plastic yielding of the material is assumed to follow the von Mises yield criterion, which is given by:

$$f = \frac{3}{2}(\boldsymbol{s} - \boldsymbol{\alpha}):(\boldsymbol{s} - \boldsymbol{\alpha}) - \sigma^2 = 0, \tag{5}$$

where f represents the yield surface, $\boldsymbol{\alpha}$ is the back stress, and σ is the radius of the yield surface that changes in the loading process.

Kinematic hardening rule

The kinematic hardening rule modified from the Ohno-Wang model [4] by Chen et al. [5] is given by:

$$\boldsymbol{\alpha} = \sum_{i=1}^{M} \boldsymbol{\alpha}_i , \tag{6}$$

$$d\boldsymbol{\alpha}_i = \gamma_i \left[\frac{2}{3} r_i d\boldsymbol{\varepsilon}_p - \left\langle \boldsymbol{n}' : \frac{\boldsymbol{\alpha}_i}{\bar{\boldsymbol{\alpha}}_i} \right\rangle^{\chi_i} \left(\frac{\bar{\boldsymbol{\alpha}}_i}{r_i}\right)^{m_i} \boldsymbol{\alpha}_i \left\langle d\boldsymbol{\varepsilon}_p : \frac{\boldsymbol{\alpha}_i}{\bar{\boldsymbol{\alpha}}_i} \right\rangle \right] , \tag{7}$$

where $\boldsymbol{\alpha}_i$ is the i-th component of deviatoric back stress $\boldsymbol{\alpha}$, $\bar{\boldsymbol{\alpha}}$ is the magnitude of $\boldsymbol{\alpha}_i$, i.e. $\bar{\boldsymbol{\alpha}}_i = \sqrt{3/2\boldsymbol{\alpha}_i : \boldsymbol{\alpha}_i}$ and $\boldsymbol{n}' = d\boldsymbol{\varepsilon}_p / dp = \sqrt{3/2}\boldsymbol{n}$, where $dp = (2/3 d\boldsymbol{\varepsilon}_p : d\boldsymbol{\varepsilon}_p)^{1/2}$. γ_i, r_i and χ_i are material constants, and m_i is an evolutionary parameter described below. The value of $< \boldsymbol{n}' : \boldsymbol{\alpha}_i / \bar{\boldsymbol{\alpha}}_i >$ are less than 1 in non-proportional loading, and can be interpreted as a measure of nonproportionality. Therefore, the term $< \boldsymbol{n}' : \boldsymbol{\alpha}_i / \bar{\boldsymbol{\alpha}}_i >^{\chi_i}$ accounts for the nonproportional loading effect on ratcheting.

For $\chi_i = 0$, equation (7) reduces to the Ohno-Wang model [4] that overpredicts multiaxial ratcheting, whereas for $\chi_i \to +\infty$, this model behaves like the Prager model [8] and predicts shakedown of ratcheting. For $0 < \chi_i < +\infty$, this model provides a compromised behavior between overprediction and shakedown.

For uniaxial loading, since $\boldsymbol{\alpha}_i$ is in the same direction as the plastic strain rate, the term $< \boldsymbol{n}' : \boldsymbol{\alpha}_i / \bar{\boldsymbol{\alpha}}_i >$ becomes unity and the multiaxial parameter χ_i is ineffective. Therefore, equation (7) reduces to the Ohno-Wang model. As a result, the proposed model generates the same uniaxial behavior as the Ohno-Wang model, so all the parameters (γ_i, r_i, m_i) of the Ohno-Wang model determined from uniaxial tests are applicable to this model without change.

The material parameters γ_i and r_i can be determined from tensile tests. For stainless steel 304 tested in this study, the values of γ_i and r_i are listed in Table 2.

TABLE 2. MATERIAL CONSTANTS USED IN THE CONSTITUTIVE MODEL

$E = 195000\text{MPa}, \nu = 0.266, \sigma_0 = 200\text{MPa}$
$\gamma_{1\sim8} = 2000,1000,500,250,167,100,62.5,31.25$
$r_{1\sim8} = 60,60,40,50,27,24,17,52\text{MPa}$
$m_{i0} = 0, \beta_i = 2.8, m_{ist} = 65, \chi_i = 8\,(i = 1 \sim 8)$
$a_p = 40,000\text{MPa}, b_p = -130\text{MPa}, c_p = 1,000$
$a_n = 45,000\text{MPa}, b_n = 300\text{MPa}, c_n = 1,000$
$c_c = 1,\ b_1 = 3,\ b_2 = 3, Q_1 = -50\text{MPa},\ r_y = 1$

In Chen et al.'s model [5], the hardening rule exponent m_i is determined by the following evolution equation:

$$dm_i = \beta_i (m_{ist} - m_i) dp , \tag{8}$$

where m_{ist} is the saturated value of m_i, which controls ratcheting rates at a later stage, and the initial value of m_i is denoted by m_{i0}, which controls the ratcheting strain during

initial cycles. β_i is the evolution coefficient that determines the evolution rate of m_i from m_{i0} to m_{ist}. These constants are determined from a uniaxial ratcheting experiment, and they are given in Table 3.

Isotropic hardening rule

The Tanaka [7] isotropic hardening rule employed here has been reported to model cyclic hardening and softening satisfactorily [6, 9, 11]. Tanaka uses a 5-dimensional plastic strain vector $\boldsymbol{E}^p$, the components of which are given by:

$$E_1^p = \varepsilon_{11}^p \quad , \quad E_2^p = 2/\sqrt{3}(\varepsilon_{11}^p/2 + \varepsilon_{22}^p) \quad , \quad E_3^p = 2/\sqrt{3}\varepsilon_{12}^p \quad ,$$
$$E_4^p = 2/\sqrt{3}\varepsilon_{23}^p, E_5^p = 2/\sqrt{3}\varepsilon_{31}^p . \qquad (9)$$

To describe the cross hardening behavior of austenitic stainless steel, he introduces a second-order tensor referred to as "structural tensor" ($\boldsymbol{C}$), the evolution of which defined by

$$d\boldsymbol{C} = c_c(\boldsymbol{u}\otimes\boldsymbol{u} - \boldsymbol{C})dp , \qquad (10)$$

where $\boldsymbol{u} = \dot{\boldsymbol{E}}^p / \left\|\dot{\boldsymbol{E}}^p\right\|$, $\otimes$ implies a tensor product, and c_c is a material constant.

The nonproportional loading parameter A is defined as

$$A = \sqrt{\frac{tr(\boldsymbol{C}^t\boldsymbol{C}) - \boldsymbol{u}\boldsymbol{C}^t\boldsymbol{C}\boldsymbol{u}}{tr(\boldsymbol{C}^t\boldsymbol{C})}} \qquad (11)$$

The yield surface radius σ is expressed as $\sigma = \sigma_o + R$, where σ_o is the initial yield stress, R is the isotropic hardening variable. Here, the evolution of R is based on the approach Aubin et al. [9] used, which is somewhat different from Tanaka [7]. R is decomposed into two parts:

$$R = R_1 + R_2 . \qquad (12)$$

The evolution equations for R_1 and R_2 are given by

$$dR_1 = b_1(Q_1 - R_1)dp , \quad dR_2 = b_2(Q_2 - R_2)dp , \qquad (13)$$

where Q_1 is treated as a material constant in [9], Q_2 is obtained from [7]:

$$Q_2 = (1-A)Q_p + AQ_n , \qquad (14)$$

where

$$Q_p = a_p q + b_p[1 - \exp(-c_p q)] ,$$

$$Q_n = a_n q + b_n[1 - \exp(-c_n q)] , \qquad (15)$$

and q is the radius of the limit surface in the plastic strain space. Q_p and Q_n are the "target values" of proportional and nonproportional hardening, respectively. The material constants a_p, b_p, and c_p are determined from uniaxial cyclic tests under strain control, and a_n, b_n, and c_n are determined from circular path tests. Finally, q is determined from:

$$q = \left\|\boldsymbol{E}^p - \boldsymbol{Y}\right\| , \qquad (16)$$

$$d\boldsymbol{Y} = r_y(\boldsymbol{E}^p - \boldsymbol{Y})dp , \qquad (17)$$

where r_y is a material constant, $\boldsymbol{Y}$ is the center of the plastic strain limit surface.

The material constants appearing in isotropic hardening rule for the test material used in this study are given in Table 2.

RESULTS AND DISCUSSION

FULLY REVERSED STRAIN CYCLING

The uniaxial tests under strain control conditions showed that the test material is cyclic softening at $\Delta\varepsilon/2$ =0.4%, and at higher strain amplitudes (1.6%, 2.0%) the material undergoes cyclic hardening. For 90° out-of-phase (circular path) tests, the material hardened even at 0.4% equivalent strain amplitude due to nonproportional hardening. At higher amplitudes in circular path tests, substantially more hardening was observed compared with uniaxial tests. Torsional cycling at the equivalent strain amplitude of 0.8% yielded cyclic softening. Regardless of cyclic hardening or softening, the stress-strain hysteresis loops stabilized as the cycles accumulated. The cyclic change of the equivalent stress is given in Fig. 3 for proportional and nonproportional loading cases. The agreement between experiment and model prediction with the material constants in Table 2 appears reasonably good. The cyclic stress-strain responses were simulated well. As an example, the axial stress vs. shear stress response for the circular path of 0.8% is given in Fig. 4.

RATCHETING UNDER UNIAXIAL LOADING AND TORSIONAL LOADING

The ratcheting strain, $(\varepsilon_{\min} + \varepsilon_{\max})/2$, from uniaxial tests is plotted in Fig. 5. The data of Test 1 and Test 2 were used to determine model constants m_{i0}, m_{ist}, β_i in Table 2 by trial and error.

The ratcheting strain under torsional loading with the same equivalent stress amplitude and mean stress as Test 1 of uniaxial ratcheting is also plotted in Fig. 5. Both predicted and experimental ratcheting strains were about the same as those of Test 1 of uniaxial ratcheting in the equivalent sense.

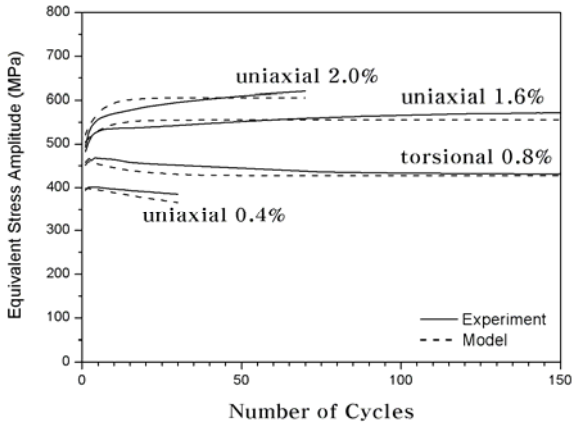

(a)

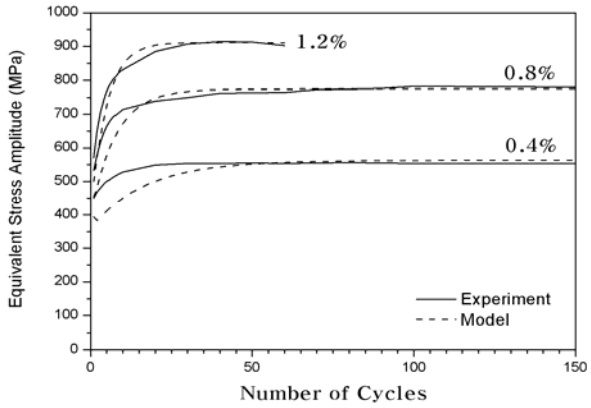

(b)

FIG. 3 VARIATION OF EQUIVALENT STRESS AMPLITUDE WITH THE NUMBER OF CYCLES: (a) UNIAXIAL AND TORSIONAL STRAIN CYCLING, (b) CIRCULAR STRAIN CYCLING

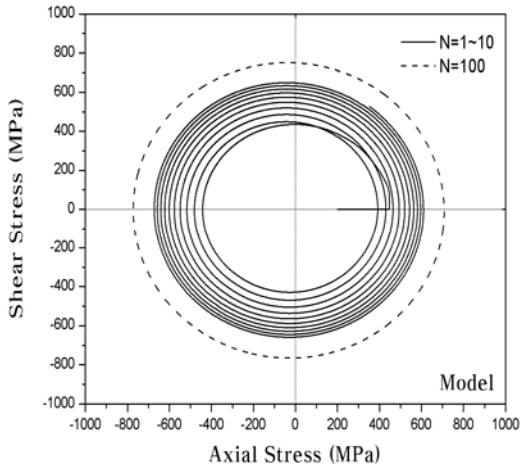

(a)

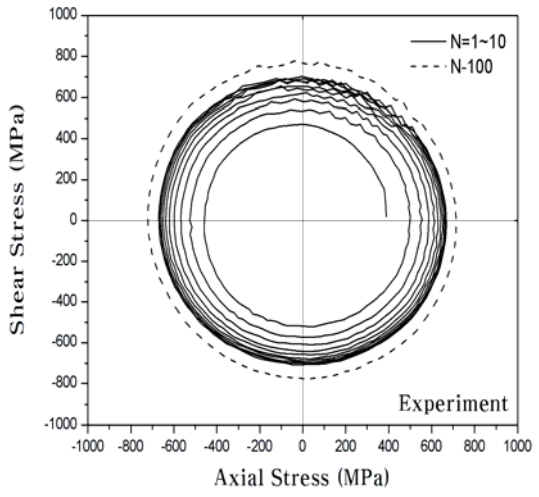

(b)

FIG. 4 EQUIVALENT AXIAL STRESS-SHEAR STRESS RESPONSE IN CIRCULAR STRAIN CYCLING WITH AMPLITUDE OF 0.8%: (a) MODEL PREDICTION, (b) EXPERIMENT

RATCHETING UNDER AXIAL-TORSIONAL LOADING

The exponent χ_i that controls the nonproportional loading effect was determined by trial and error such that the selected value provides a similar level of correlation for the cases considered. The experimental results and model predictions for ratcheting strain are reviewed in the following for each case.

The loading path for Case 1 is shear strain cycling with constant axial stress. This is a widely adopted loading path for studying multiaxial ratcheting. Two tests were conducted with axial stresses of 150MPa and 100MPa. The experimental and predicted ratcheting strains are compared in Fig. 6(a). The model prediction and experimental data are close for Test 2, but there were considerable differences in ratcheting rates for Test 1 at larger cycles.

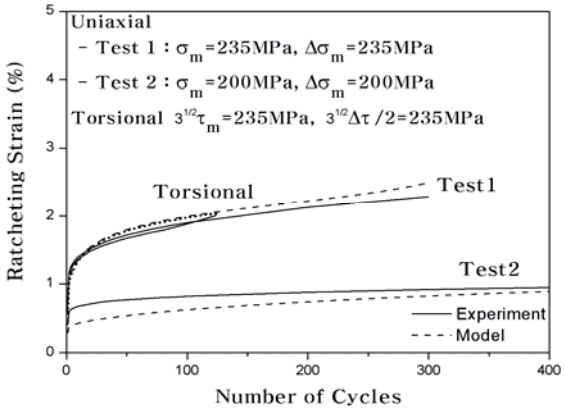

FIG. 5 RATCHETING STRAIN UNDER UNIAXIAL LOADING AND TORSIONAL LOADING

Case 2 is an inclined linear path of positive slope with a fully reversed torsional strain cycle and an axial stress cycle with mean stress. As seen in Fig. 6(b), the model predictions are larger than the experimental values, particularly for Test 1. The axial and torsional hysteresis loops were similar to those of a uniaxial ratcheting test and a fully reversed shear strain control test, respectively.

Case 3 is a circular path where the axial stress and torsional strain are 90°-out-of-phase. The ratcheting strain is plotted in Fig. 6(c). The model overpredicts ratcheting but the rate of ratcheting at larger cycles looks satisfactory. The maximum equivalent stress versus cycle is plotted in Fig. 7. It is found that the material softens significantly. This is due to the fact that the effect of softening at low strain amplitudes, both in the axial and shear directions, dictates the nonproportional hardening effect. In fact, similar cyclic softening behavior was observed in all axial-torsional ratcheting tests to different extents. The predicted curve also yields the cyclic softening behavior but at a somewhat lower stress level throughout.

Case 4 is a bowtie path which can be viewed as a combination of two inclined paths with increasing axial stress, each connected by a decreasing axial stress path with torsional strain kept constant. The axial stress is cycled twice for a torsion cycle, while each axial cycle corresponds to one torsion cycle in Case 2. Therefore it is reasonable to anticipate that the accumulation of plastic strain will be substantially larger than Case 2 (Corona et al. [10]). The ratcheting strain for Case 4 is actually found to be considerably larger as shown in Fig. 6(d). The simulated ratcheting strain was lower than the experimental, and it tends to lead to a shakedown state while the experimental data shows steady increase. The axial vs. torsional stress trajectory showed symmetry with respect to τ = 0, which the model predicted adequately as shown in Fig 8(a), (b). The axial vs. shear strain loops are also given in Fig 8(c), (d). The equivalent stress versus cycle plot shows cyclic hardening more than Case 3 in the first 50 cycles followed by slow softening; see Fig 7. This phenomenon was simulated in the analysis, though the initial stress at low cycles did not go up as much as the experimental stress. The less initial hardening may be related to the delayed initial hardening trend of the isotropic model found in Fig 3 at low strain amplitudes before the softening mechanism becomes more active. It is also noted that larger additional hardening in some bowtie paths than in circular paths is also found in Calloch and Marquis [11] for stainless steel 316.

Case 5 is a reverse bowtie path that was generated by reversing the direction of loading in Case 4. Other than the direction, loading conditions are the same, and therefore these two cases will manifest the effect of direction of loading path on the ratcheting strain. As in Case 4, one shear strain cycle and two axial cycles are involved in this path. The ratcheting strain was much smaller compared with Case 4. The model predicted this phenomenon properly; see Fig. 6(e). The axial stress-shear stress trajectory was again symmetric with respect to τ = 0. These features were well duplicated in model results. The equivalent stress vs. cycle plot showed less initial hardening and slightly more follow-up softening compared with Case 4; see the experimental curves of Fig. 7. It may be expected that more ratcheting will occur in Case 5 than in Case 4 in view of more cyclic softening. The reverse was true, however, in the present results. It is apparent that the loading path direction is much more influential on ratcheting than cyclic changes of the material. From the modeling perspective, the two paths give rise to different angles between the direction of the yield surface translation and the direction of deviatoric stress increment, thus giving rise to different degrees of kinematic hardening responsible for different ratcheting behavior. Similar observations of ratcheting for bow-tie paths can be found in literature for other materials [5, 10].

Case 6 is different from other cases in that the axial cycle was a fully reversed strain cycle and the torsional stress was kept constant. The equivalent stress and strain levels were the same as Test 2 of Case 1. Ratcheting in this case occurs in shear strain. The equivalent ratcheting strain predicted by the model is compared with experimental results in Fig. 6(f). The prediction shows ratcheting strain develops early and then reaches a near-shakedown value, while the experiment shows continuous increase. An interesting point is that the ratcheting strain is close to that of Test 2 of Case 1. This is consistent with the similarity of uniaxial and torsional ratcheting data obtained under the same equivalent stress as shown in Fig. 5.

In summary of the results of the 6 cases, it may be said that the constitutive model has a potential to provide acceptable prediction of ratcheting strain under various loading conditions. The evolution of the exponent m_i in the nonlinear kinematic hardening rule and the introduction of an additional

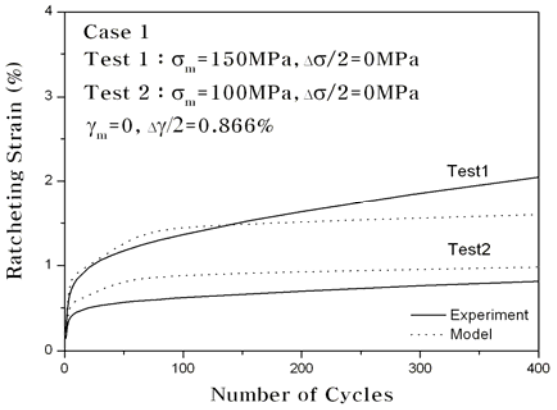

(a)

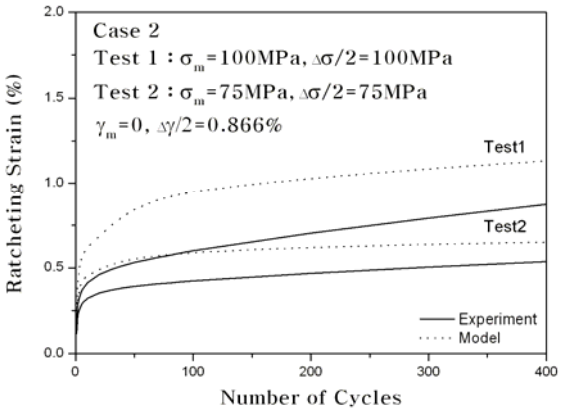

(b)

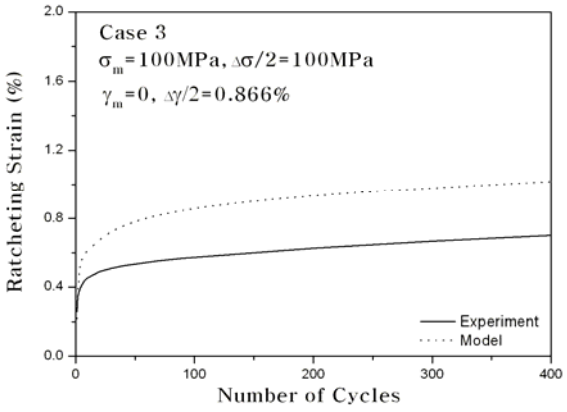

(c)

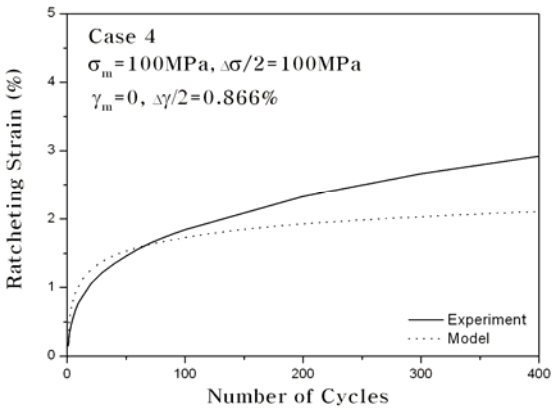

(d)

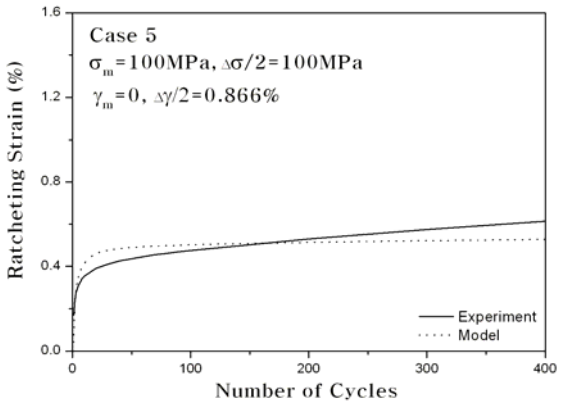

(e)

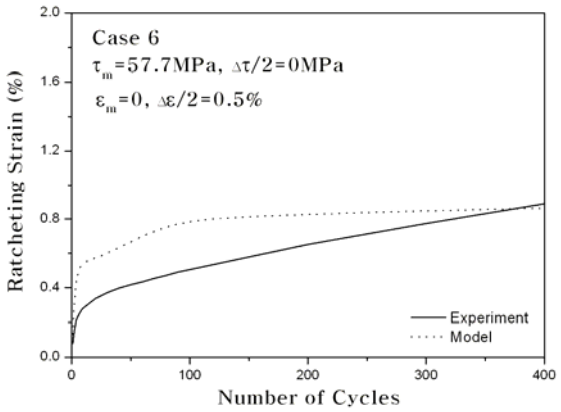

(f)

FIG. 6 COMPARISON OF PREDICTED AND EXPERIMENTAL RATCHETING STRAINS FOR AXIAL-TORSIONAL CYCLES

nonproportionality parameter χ_i appear to help resolve the persistent overestimation problem of ratcheting strain under multiaxial loading. However, in many of the loading cases considered in this study, the constitutive model with selected material constants tends to produce an overestimation of ratcheting strain in the early phase and a near-shakedown state in the later stage where experimental data show continued increases. This could lead to substantial underestimation of the ratcheting strain over a longer period unless the actual ratcheting rates decrease fast enough. Thus, the values of χ_i and m_i will have to be changed for better agreement in the longer range of cycles. In fact, many trial runs indicated that reducing the values of m_i along with increasing the constant β_i makes the ratcheting rate to increase in larger cycles. In the meantime, this also causes considerable overestimation of uniaxial ratcheting and multiaxial ratcheting for some loading paths in the range of 400 cycles.

CONCLUSIONS

The ratcheting behavior at relatively low cycles is thought to be influenced by isotropic hardening behavior of the material. Consequently, the Ohno-Wang kinematic hardening rule modified by Chen et al. [5] was extended to include Tanaka's isotropic hardening model. The constitutive theory was then applied to simulate the ratcheting behavior of stainless steel 304 tested under uniaxial, torsional and nonproportional axial-torsional loading. The results show that the constitutive model can curb the overestimation problem of multiaxial ratcheting. However, the model still needs further improvement in controlling the rate of ratcheting over an extended number of cycles.

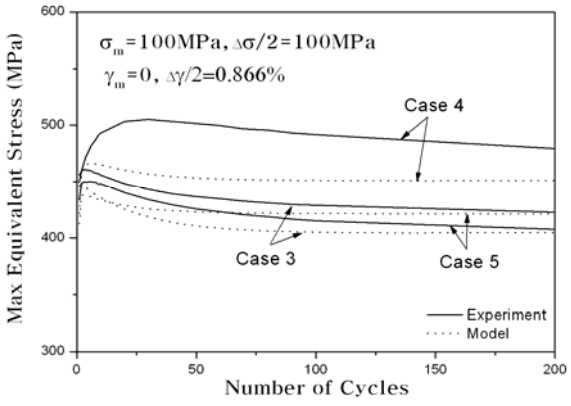

FIG. 7 VARIATION OF MAXIMUM EQUIVALENT STRESS WITH CYCLES FOR CASE 3, CASE 4 AND CASE 5

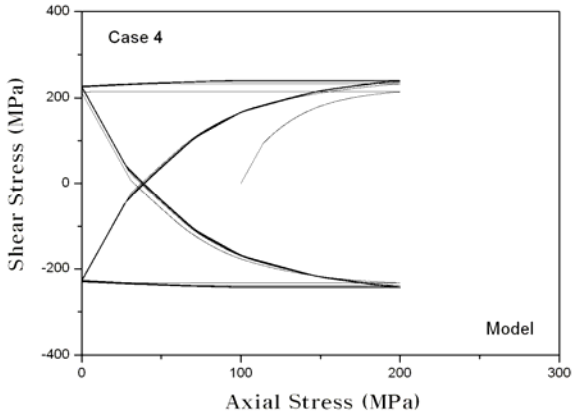

(a)

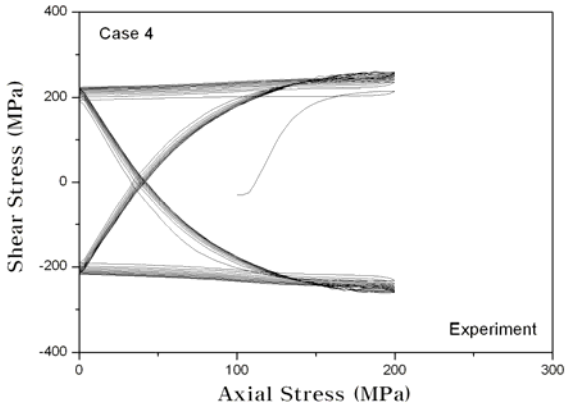

(b)

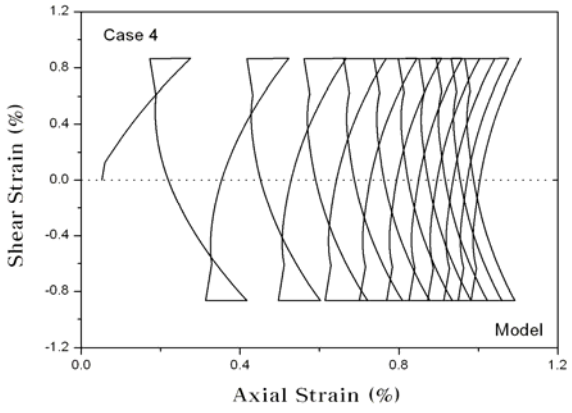

(c)

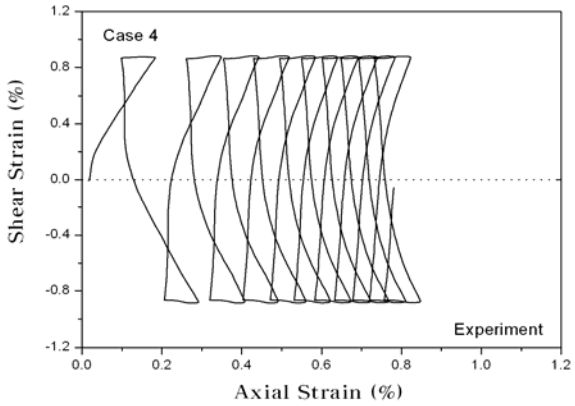

(d)

FIG. 8 COMPARISON OF CASE 4 STRESS AND STRAIN RESPONSES BETWEEN MODEL PREDICTION AND EXPERIMENT: (a),(b) AXIAL STRESS-SHEAR STRESS RESPONSE; (c),(d) AXIAL STRAIN-SHEAR STRAIN RESPONSE

ACKNOWLEDGMENTS

The first two authors (KSK, RJ) gratefully acknowledge financial support for this work from the Brain Korea 21 Program and an internal R&D program of Mechanical Engineering Department of Pohang University of Science and Technology.

REFERENCES

[1] Bari, S., and Hassan, T., 2000, "Anatomy of coupled constitutive model for ratcheting simulation," International Journal of Plasticity, **16**, p. 381.

[2] Bari, S., and Hassan, T., 2002, "An advancement in cyclic plasticity modeling for multiaxial ratcheting simulation," International Journal of Plasticity, **18**, p. 873.

[3] Armstrong, P.J., and Frederick, C.O., 1966, "A mathematical representation of the multiaxial Bausinger effect," CEGB Report No. RD/B/N 731.

[4] Ohno, N., and Wang, J.-D., 1993, "Kinematic hardening rules with critical state of dynamic recovery, part I: formulations and basic features for ratcheting behavior," International Journal of Plasticity, **9**, p. 375.

[5] Chen, X., Jiao, R., Kim, K.S., 2005, "On the Ohno-Wang kinematic hardening rules for multiaxial ratcheting modeling of medium carbon steel," International Journal of Plasticity, **21**, p. 161.

[6] Calloch, S., and Marquis, D. 1999, "Triaxial tension-compression tests for multiaxial cyclic plasticity," International Journal of Plasticity, **15**, p. 326.

[7] Tanaka, E., 1994, "A nonproportional parameter and a cyclic viscoplastic constitutive model taking into account amplitude dependences and memory effects of isotropic hardening," European Journal of Mechanics, A/Solids, **13**, p. 155.

[8] Prager, W., 1956, "A new method of analyzing stresses and strains in work hardening plastic solids," ASME Journal of Applied Mechanics, **23**, p. 493.

[9] Aubin, V., Quaegebeur, P., and Degallaix, S.,2003, "Cyclic behavior of a duplex stainless steel under multiaxial loading: Experiment and Modelling," ESIS STP Biaxial/Multiaxial Fatigue and Fracture, p. 401.

[10] Corona, E., Hassan, T., and Kyriakides, S., 1996, "On the performance of kinematic hardening rules in predicting a class of biaxial ratchetting histories," International Journal of Plasticity, **12**, p. 117.

[11] Calloch, S., and Marquis, D. 1997, "Additional hardening due to tension-compression non-proportional loadings: Influence of loading path shape," ASTM STP 1280, ASTM, p. 113.